

A detailed investigation of ambient aerosol composition and size distribution in an urban atmosphere

S. Levent Kuzu · Arslan Saral · Selami Demir ·
Gülsüm Summak · Göksel Demir

Received: 8 May 2012 / Accepted: 27 August 2012 / Published online: 12 September 2012
© Springer-Verlag 2012

Abstract This research was executed between March 2009 and March 2010 to monitor particulate matter size distribution and its composition in Istanbul. Particulate matter composition was determined using ion chromatography and inductively coupled plasma optical emission spectrometry. The sampling point is adjacent to a crowded road and the Bosphorus Strait. Two prevailing particulate modes are found throughout PM₁₀ by sampling with a nine-stage low-volume cascade impactor. First mode in the fine mode is found to be between 0.43 and 0.65 μm, whereas the other peak was observed between 3.3 and 4.7 μm, referring to the coarse mode. The mean PM₁₀ concentration was determined as 41.2 μg/m³, with a standard deviation of 16.92 μg/m³. PM_{0.43} had the highest mean concentration value of 10.67 μg/m³, making up nearly one fourth of the total PM₁₀ mass. For determining the effect of traffic on particulate matter (PM) composition and distribution, four different sampling cycles were applied: entire day, nighttime, rush

hour, and rush hour at weekdays. SO₄⁻² and organic carbon/elemental carbon proportions are found to be lower in night samples, representing a decrease in traffic. The long-range transports of dust storms were observed during the sampling periods. Their effects were determined analytically and their route models were run by the HYSPLIT model and validated through satellite photographs taken by the NASA Earth Observatory.

Keywords Particulate matter · Size distribution · Ion and elemental composition · Long-range transport

Introduction

Particulate matter (PM) in the urban atmosphere has been of concern to air pollution engineers. PM sampling has improved gradually from the 1970s. Earlier PM measurement techniques comprised total suspended particulate sampling. Since then, the sampling procedures were modified considering the impact of PM on human health. Ambient air quality standards include PM₁₀ threshold limits, which led to the start of PM₁₀ sampling.

For a better understanding of PM issues, cascade impactors are used to resolve the particulate matter according to their aerodynamic diameters, especially in health-related researches. Since atmospheric PMs are composed of various solid or liquid components, being a complex matrix, they have different physical and/or chemical characteristics (Perrino et al. 2011).

Different sources cause discrete aerosol size distributions. Whitby et al. (1975) illustrated the trimodal structure of atmospheric aerosol number size distribution as nuclei, accumulation, and coarse particle. However, under most circumstances, this distribution appears to be bimodal (Morawska et al. 1999). Coarse mode particulate matter usually occurs as a

Responsible editor: Philippe Garrigues

S. L. Kuzu (✉) · A. Saral · S. Demir · G. Summak
Civil Engineering Faculty, Environmental Engineering
Department, Yildiz Technical University,
34220 Davutpaşa-Esenler, Istanbul, Turkey
e-mail: skuzu@yildiz.edu.tr

A. Saral
e-mail: saral@yildiz.edu.tr

S. Demir
e-mail: seldemir@yildiz.edu.tr

G. Summak
e-mail: gulsum_borucu@hotmail.com

G. Demir
Engineering Faculty, Environmental Engineering Department,
Bahcesehir University,
34538 Besiktas, Istanbul, Turkey
e-mail: goksel.demir@bahcesehir.edu.tr

consequence of mechanical processes, like soil dust, cloud droplets, and biological particles (Seinfeld and Pandis 1997), whereas the fine mode emerges as a result of a homogenous or heterogeneous nucleation from gas to particle conversion and anthropogenic pollution due to combustion (Hewitt and Jackson 2009).

In urban areas, traffic is responsible for more than 50 % of ambient particulate matter (Wrobel et al. 2000). Traffic-related particulate emissions are enriched with trace elements (Hlavay et al. 1992; Fernandez Espinosa et al. 2001). Some most prominent constituents are summarized as follows: Sb and Cu are from brake-lining materials (Huang et al. 1994), Zn from tire tread (Adachi and Tainosho 2004), and Cr from fuel combustion (Xia and Gao 2011). Al-Khashman (2004) expressed that street dust is a significant contributor to urban environment; the stated main contributors in his study were Fe, Cu, Zn, Ni, and Pb.

A great number of research concerning epidemiological issues have been performed on particulate matter so far. These studies show that a high particulate concentration, especially in the fine mode, has detrimental effects on human health. These pollutants trigger respiratory and cardiovascular diseases; they also have detrimental effects on the nervous system and cause cancer and premature death (EPA 2010; Vedal 1997). Inflammation on the epithelial surfaces of the lung was also reported (Dockery et al. 1989; Harrison and Yin 2000; Poschl 2005).

On the other hand, particulate matter having an aerodynamic diameter $<2.5 \mu\text{m}$ scatter and absorb light, which causes a reduction in visibility (Brewer and Belzer 2001). Jacob (1999) expressed that if the aerosols were absent in the atmosphere, visual range would be 300 km, which is limited by the scattering of air molecules. Cheng and Tsai (2000) stated that visibility distance is 8–10 km in urban areas, while that distance is approximately 25–30 km in remote areas.

For determining the particle size distribution and characterizing the ion and elemental composition of airborne particles, a cascade impactor has been used from March 2009 until March 2010. Na, K, Ca, Mg, V, Co, Ni, Zn, Al, Cd, Cr, Pb, Fe, and Mo were analyzed using inductively coupled plasma optical emission spectrometry (ICP-OES; Perkin Elmer, Optima 7000). Anions and cation of SO_4^{2-} , NO_2^- , NO_3^- , Br^- , Cl^- , F^- , and NH_4^+ were analyzed using an ion chromatography instrument (Dionex, ICS-3000).

A great number of papers have been published up to this date, dedicated to determine ambient PM concentrations and to resolve the chemical composition of $\text{PM}_{10}/\text{PM}_{2.5}$. However, the current literature lacks papers concerning PM size-resolved chemical analysis, especially in Turkey. This research is essential to providing detailed information of species through different cutoff diameters. The concentrations

detected in different stages would also support further source identification studies.

Materials and methods

Site description

Sampling was done within the Besiktas Campus of Yildiz Technical University (YTU, Turkey) near a connection road between Barbaros Avenue and the Bosphorus Bridge through O-1 Highway. These roads are shown in different colors in Fig. 1. Barbaros Avenue, O-1 Highway, connection road, and the sampling zone are depicted in yellow, green, gray, and black, respectively. Istanbul is the most crowded city of Turkey, with a population of over 13 million people. Istanbul constitutes about 18 % of all Turkey's population (TUIK 2011). The Bosphorus Strait divides the city into two sides: the Asian and European sides. The Asian side mostly hosts residential areas, while commercial and industrial activities concentrate on the European side. Transportation between the two sides is accomplished via sealines and the two bridges. These two bridges together offer a total of 14 lanes. Therefore, dense traffic is observed especially at rush hours, with as low as 5–6 km/h of fleet velocities. The air quality around the sampling site, being located near these roadways with extremely high traffic loads, is considered to be under great influence of traffic-related emissions.

Sampling and analysis

A Mark II Andersen cascade impactor was used to separate particulate matters according to their sizes. The sampler includes eight particulate collecting stages. Each impactor stage contains multiple precision-drilled orifices. When air passes through the sampler, multiple jets of air flow in each stage direct any airborne particles toward the surface of the collection plate for that stage, where a filter is present above. The size of the jets is constant for each stage, but is smaller in each succeeding stage. In this way, in each succeeding stage, air is drawn through the orifices faster. Whether a particle is impacted on any given stage depends on its aerodynamic dimension. Any uncollected particle on the first stage follows the air stream around the edge of the plate to the next stage, where it is either impacted or passed on to the succeeding stage, and so until the jet velocity is sufficient for impaction. Each of the nine stages has cutoff diameters of 9.0, 5.8, 4.7, 3.3, 2.1, 1.1, 0.65, 0.43, and $<0.43 \mu\text{m}$ in the collection order. The last stage emphasizes a backup filter.

The cascade impactor was placed at about 10 m away from the connection road between Barbaros Avenue and

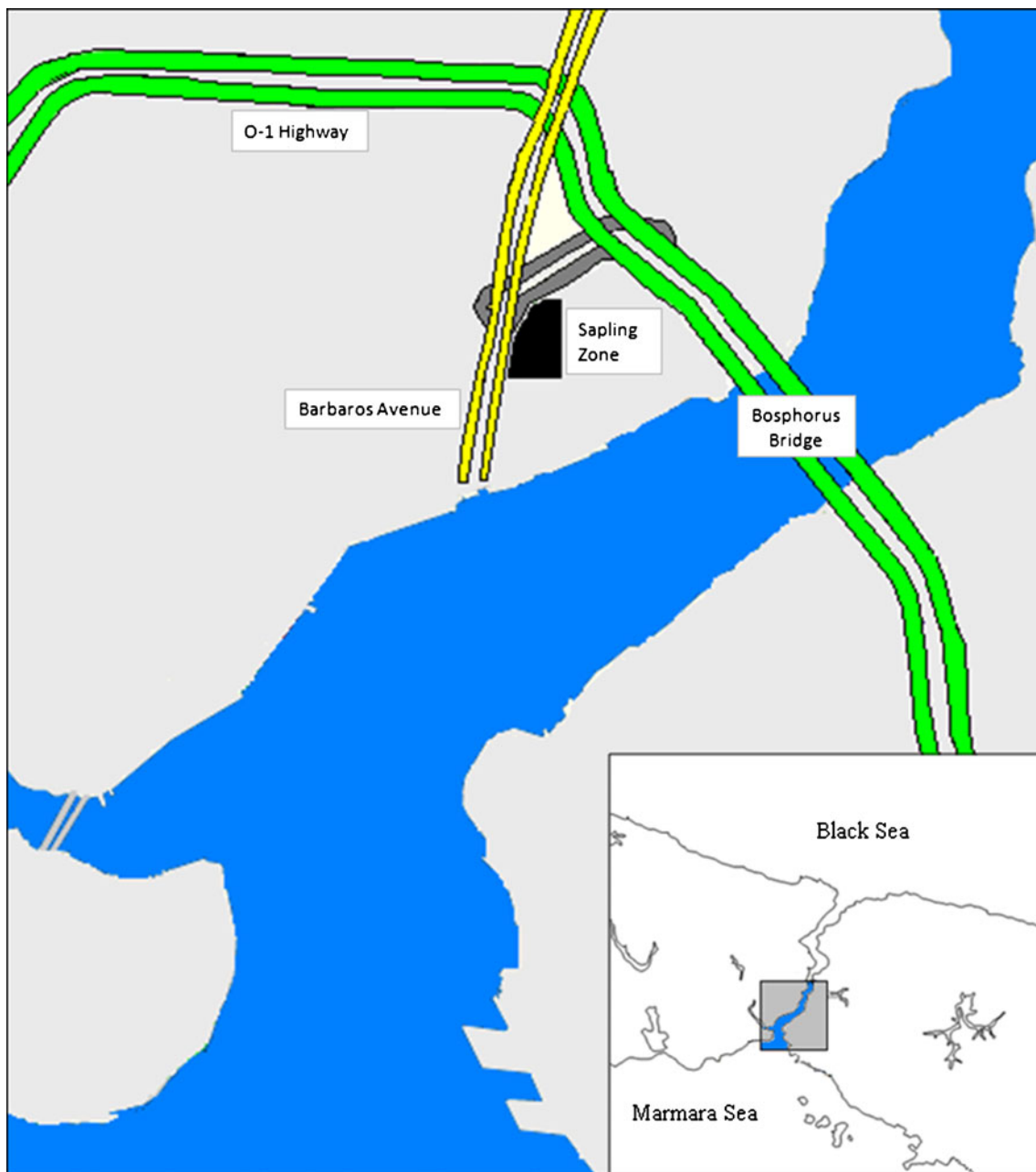


Fig. 1 Study area and sampling zone

Bosphorus Bridge. The samples were collected through four different time cycles to monitor diurnal changes of the concentration and composition of particulate matter. These cycles are shown in Table 1. In the first cycle, each sequence was run for 1 week to acquire enough particulate mass for analysis. The second cycle was the nighttime cycle (2230 to 0630 hours) to observe the ambient concentrations during a reduced traffic emission input. In the third cycle, sampling was accomplished between 0630–1030 and 1630–2030 hours. The fourth cycle was the same as the third one, except the sampling

was not performed during weekends and the samples represented only weekday conditions. The entire sampling was executed for a 1-year period.

A significant variation between cycles 3 and 4 was not observed from both the concentration and composition perspectives. For that reason, these two cycles are shown as one, as rush hour in the subsequent sections.

Quartz filters were used to collect all particle samples. At first, filters were dried at 103 °C in an oven followed by stabilization at constant temperature (20 ± 2 °C) and relative humidity (50 ± 2 %) for 2 days. When the sampling process

Table 1 Sampling periods

Cycle	Sampling period	Operation hours in 1 day	Days of the week	Sampling date
1	All day	24 h	All days	25.02.09–01.09.09
2	Night time	2230–0630 hours	All days	01.09.09–03.11.09
3	Rush hour	0630–1030 hours 1630–2030 hours	All days	03.11.09–05.01.10
4	Rush hour	06:30–10:30 hours 16:30–20:30 hours	Weekdays	05.01.10–02.03.10

was completed, filters were re-stabilized under the same conditions, except the drying operation, in order not to lose condensable particulate matter fraction. All filters were weighed before and after sampling via an analytical balance (AND GR202) with a reading precision of 10 µg. The weight differences between tare and the sampled filters were recorded and all of them were divided by the total collected mass for mass frequencies. These frequencies were then summed up sequentially for cumulative values. These cumulative values were plotted on a log-probability paper.

To dissolve the elements which were captured on the particle surface into the liquid phase, a microwave digestion method is developed. As a starting point, Upadhyay et al. (2009) have suggested a mixture of acids and H₂O₂ for the extraction of trace elements collected on quartz filters. This mixture included 10 ml HNO₃, 1 ml HF, and 4 ml deionized water. The digestion process was performed on three steps of heating the mixture up to 140, 170, and 180 °C, respectively. The digestion operation takes 60 min to complete in this procedure. The recoveries of elements were checked with SRM 2709 and 1649a. Unfortunately, this digestion procedure was unsuccessful in our study. According to our optimization studies, optimum digestion occurred when 4.4 ml HNO₃, 1.1 ml H₂O₂, and 0.6 ml HF were utilized using a Berghof MWS-3-type microwave digestion device. A five-step digestion procedure was appointed, which consists of 5 min of heating from 100 to 140 °C and a 10-min hold at this temperature; heating up to 175 °C at a rate of 7 °C/min and 10-min hold; then heating up to 195 °C at a rate of 4 °C/min and keeping this temperature for 15 min; and, finally, cooling down to 100 °C in 5 min and waiting again for 5 min at that temperature. A total of 60 min was spent for the digestion procedure. Then, the liquid phase is diluted with deionized water and filtered to a 50-ml Falcon tube to proceed to the next step of ICP analysis. ICP-OES was used to analyze the Na, K, Ca, Mg, V, Co, Ni, Zn, Al, Cd, Cr, Pb, Fe, and Mo contents of ambient particulate matter.

The other part of the filter was used with a different type of extraction method to dissolve water-soluble ions. Each filter was put into a flask; 50 ml of deionized water having a resistivity value of 18.2 MΩ/cm was added. For the dissolution of water-soluble ions, flasks

were put into a shaker unit and were shaken for 24 h. The final solution was filtered and the NH₄⁺, F⁻, Cl⁻, NO₂⁻, NO₃⁻, Br⁻, and SO₄⁻² concentrations determined using ion chromatography.

The recovery results were within 5 % of the certified amount. The analytical relative standard deviation was ≤3 % for the majority of the elements in three replicates. The limit of detection (LOD) values were calculated as blank average plus three times the standard deviation. The LOD values determined for each element ranged from 0.4 to 18 ng/m³. All results were blank-corrected.

Meteorological conditions

In Table 2, the monthly meteorological conditions are summarized during the sampling period. Mixing height values were taken from the ARL archived meteorological data of the NOAA (Air Resources Laboratory 2012).

The calculated mean mixing heights considering the sampling hours for three different sampling periods were 737, 330, and 530 m for the entire day sampling, nighttime sampling, and rush hour sampling, respectively.

Table 2 Meteorological conditions during the sampling period

Sampling month	Temperature (°C)			Wind		Precipitation Total (mm)	Mixing height (m)
	Min	Avg	Max	Speed (m/s)	Direction		
1	5.9	8.7	12.1	1.7	WSW	76.5	524
2	8.5	11.5	16.1	2.8	NNE	14.0	526
3	14.7	18.3	23.1	2.5	NNE	8.6	707
4	19.7	23.7	28.7	1.9	NE	4.3	772
5	21.9	25.3	29.7	3.2	NNE	16.0	917
6	21.0	24.0	28.1	4.0	NE	3.8	974
7	18.0	21.3	26.5	2.7	NNE	34.0	682
8	15.3	17.9	22.3	2.2	N	26.7	492
9	11.6	13.2	19.7	1.3	SW	30.7	342
10	7.3	10.4	16.6	1.9	SW	51.3	445
11	4.3	6.8	9.3	1.9	N	84.3	557
12	5.5	8.7	12.3	1.5	N	65.8	548

Results and discussion

Gravimetric analysis results

Ambient concentrations of particulate matter in the given size ranges were measured gravimetrically. Table 3 summarizes the measurement results.

PM sampling was carried out for at least a 7-day period in order to collect enough particulate matter for the analysis of metal and ion compositions. However, by this sampling procedure, it is almost not possible to observe peak values which may occur in some short time intervals; rather, only the weekly individual average value is available. Considering Table 3, incremental trends of the PM concentrations with decreasing diameter could be observed. The particle range is not uniform throughout the stages. To clearly investigate the modality, $dC/d\log D_p$ versus diameter graphs were prepared along with log-probability graphs. In Fig. 2, the modality of ambient PM is shown.

There are two prevailing modes, as expected, in an urban atmosphere. One peak is observed at $0.65 \mu\text{m}$, in the fine mode, referring to the potential traffic source. Another peak is at $4.7 \mu\text{m}$. The latter peak is in coarse mode and consists of mechanically generated particles. As accurate peak concentration values in a short period cannot be obtained, statistical analyses were performed to make a more realistic evaluation.

In Fig. 3, the PM concentration values were classified according to the impactor cutoff diameters. Each size group has three different periods: the entire day, night hours, and rush hours, respectively. The vertical line inside the box refers to the median value, where the left and right ends of the box show 25 and 75 %, respectively. The whiskers on the left- and right-hand sides show the minimum and maximum observed values, respectively.

Larger fluctuations of ambient concentrations were detected for particles smaller than $0.43 \mu\text{m}$. Nighttime samples did not deviate as the daytime samples did. The reason

Table 3 Weekly ambient PM concentration (in micrograms per cubic meter) for different PM sizes

Particle size range (μm)	Mean	$\pm\text{SD}$	Min	Median	Max
10–9	0.75	0.79	0.07	0.76	2.75
9–5.8	2.40	1.52	0.34	2.12	5.29
5.8–4.7	3.81	4.08	0.45	2.15	16.54
4.7–3.3	4.73	4.84	0.54	4.03	21.69
3.3–2.1	4.07	1.81	1.30	3.79	8.24
2.1–1.1	4.40	2.01	0.81	4.53	8.95
1.1–0.65	4.83	2.67	1.44	4.16	13.63
0.65–0.43	5.25	2.13	1.14	4.95	9.12
<0.43	10.67	6.49	3.60	8.11	29.17
<10	41.12	16.92	17.10	40.06	92.60

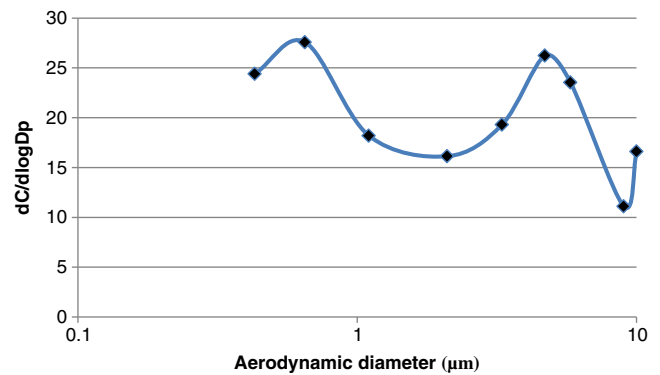


Fig. 2 Modality of ambient PM with continuous sampling for 1 week

for that was a constant low-density traffic load which is observed at the connection road during nighttime. It is clearly observed in the figure that particles between 5.80 and $9.00 \mu\text{m}$ and between 0.43 and $1.10 \mu\text{m}$ show higher differences than the other sizes when comparing nighttime and rush hour concentrations. This higher difference suggests a vehicle origin for these particle sizes. Fine particles between 0.43 and $1.10 \mu\text{m}$ mostly originate from traffic emissions and then coarse particles from mechanical abrasion of the road pavement.

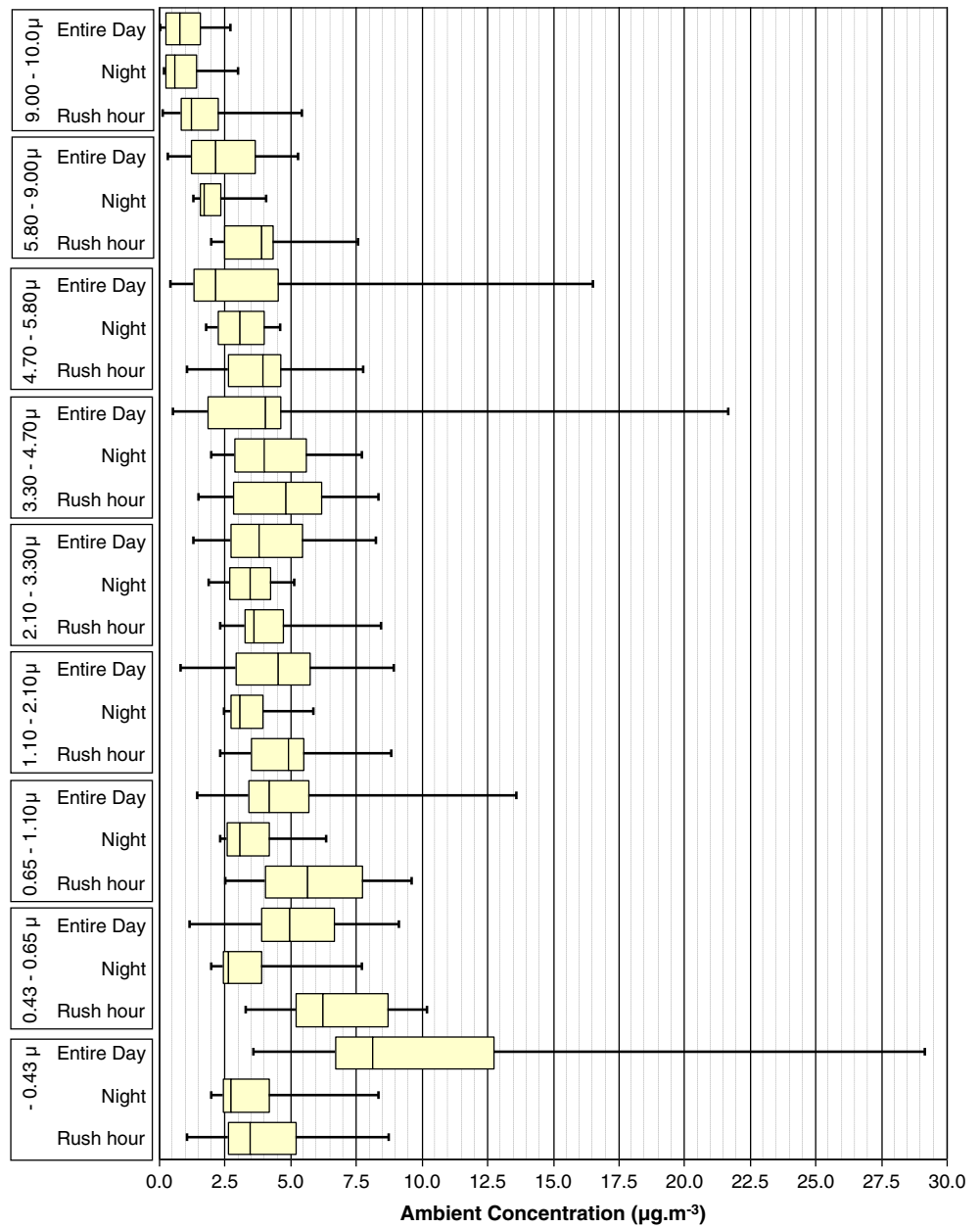
Figure 4 shows the PM_{10} concentrations. Although this figure is less informative than Fig. 3, the figure is plotted for evaluating air quality standards which are based on PM_{10} sampling. Therefore, supplying information on a PM_{10} basis is also essential to make comments on the threshold limits.

To calculate the PM_{10} value using a cascade impactor, theoretical impaction curves are used, which are provided by the impactor manufacturer. The same methodology is also followed by Hieu and Lee (2010) to determine PM_1 , $\text{PM}_{2.5}$, PM_4 , and PM_{10} concentrations. According to this method, all fractionated mass values are added to each other, excluding the stage between 9 and $10 \mu\text{m}$. The mass of this stage is added to succeeding stages by multiplying 0.78 , which is the correction factor corresponding to PM_{10} .

Night samples showed the lowest concentration values, as expected. But a high deviation was observed. This is because of the sampling procedure applied at night sampling. As a low-volume cascade impactor was used, a prolonged sampling period was applied. Otherwise, it would not be possible to collect enough particulate mass for chemical analysis.

The maximum median concentration was observed during the rush hour sampling period, as expected. If the mixing height value of the atmosphere is taken into account for the correction of different seasonal and diurnal properties, it would be seen that the night PM_{10} concentration must be lower than it was and the rush hour PM_{10} concentration must be higher than it was. During the entire day sampling, two long-range dust transportations occurred from the Saharan Desert and the Arabian Peninsula. That is why the

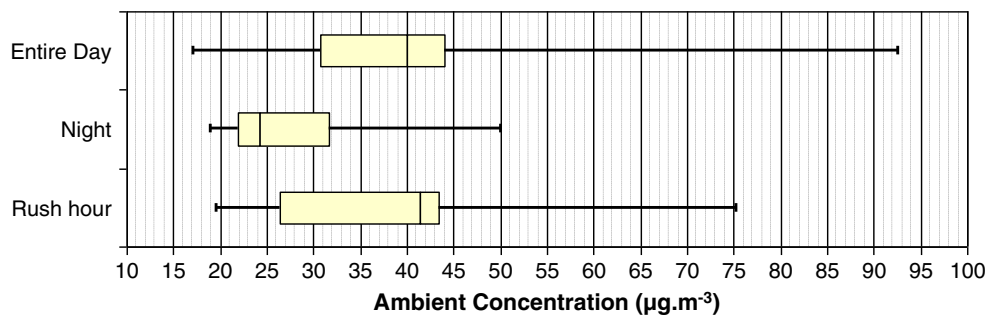
Fig. 3 Box-whisker plots of PM concentration according to size and sampling periods



highest concentration was observed during the entire day sampling. Another transportation occurred during the rush hour sampling from the Saharan Desert.

Turkish NAAQS was revised in 2008. Until the revision, the threshold value for PM₁₀ was 300 µg/m³. After that revision, the threshold value is to be reduced

Fig. 4 PM₁₀ concentration box-whisker plots



to $100 \mu\text{g}/\text{m}^3$ by equal interval values each year until 2014. The acquired PM_{10} concentrations are well below the current limit value. The ultimate threshold concentration is going to be reached in 2019, which is $50 \mu\text{g}/\text{m}^3$. Statistical plots show that $50 \mu\text{g}/\text{m}^3$ would exceed by 16 %, in the current case.

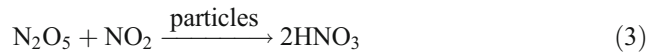
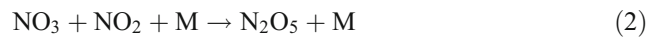
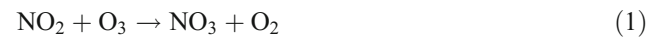
Chemical composition

The ionic and metallic constituents of ambient aerosols were investigated to obtain detailed information on the aerosol composition. The results of the ion and metal analyses are summarized in Figs. 5, 6 and 7, showing respectively the entire day, night, and rush hour sampling box–whisker plots.

Na and Ca are abundant through all the sampling periods. Other dominating constituents are K, Mg, Al, Zn, Cl^- , NO_3^- , and SO_4^{2-} . SO_4^{2-} and NO_3^- are principally present due to combustion sources. Nighttime and rush hour samples were collected during the fall and winter seasons, while entire day samples were collected in spring and summer. Thus, elevated values of NO_3^- and SO_4^{2-} are observed in Figs. 6 and 7.

SO_4^{2-} concentration is somewhat higher during the rush hour sampling than during the nighttime sampling, while NO_3^- is significantly higher during nighttime. A higher sulfate concentration at daytime is potentially due to higher insulation conditions which oxidize SO_2 . During daytime, NO_2 is reduced in the atmosphere by many different reactions. Finlayson-Pitts and Pitts (1993) stated that Eq 1, which results in the formation of the

nitrate radical (NO_3), provides a major nighttime source of HNO_3 .



Also, NO_2 reacts with the OH radical to form HNO_3 . The saturation vapor pressure of HNO_3 is high. As a consequence, HNO_3 condenses onto existing aerosols such as sea salt or alkaline mineral aerosols. Sulfate can condensate onto mineral particles or can be oxidized inside cloud droplets containing sea salt. Both are referred to as heterogeneous nucleation, and these compounds could react with NH_4^+ that is readily present in the atmosphere to form secondary aerosols. It is beneficial to look for the NH_4^+ level to prove ammonium sulfate and ammonium nitrate particle formation from the gas phase. The highest NH_4^+ levels were observed below $1 \mu\text{m}$, especially between 0.43 and $0.65 \mu\text{m}$. The maximum concentration for NO_3^- was reached below $0.43 \mu\text{m}$.

Sea salt aerosol is produced by the bursting of air bubbles resulting from the entrainment of air induced by wind stress along the seashore (O'Dowd et al. 1997) and transported inland by wind. Bigger particles can be carried longer distances before they settle due to high wind speeds, and this speed can also lead to an increase in the salt concentration in generated aerosols (Gustafsson and Franzen 1996). Our

Fig. 5 Box–whisker plot of chemical species of the entire day samples

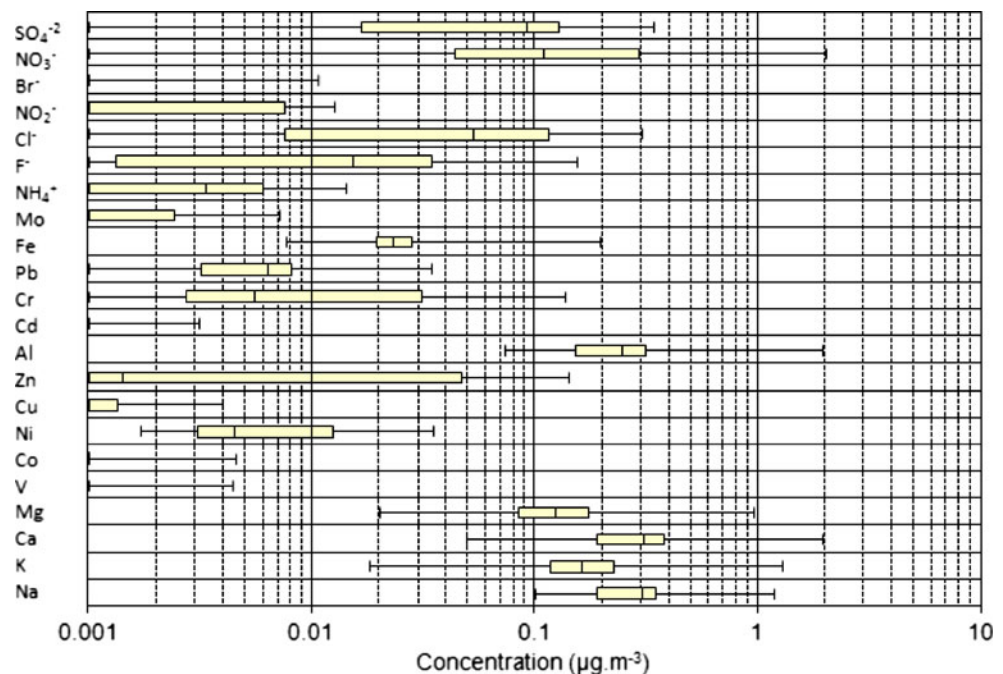
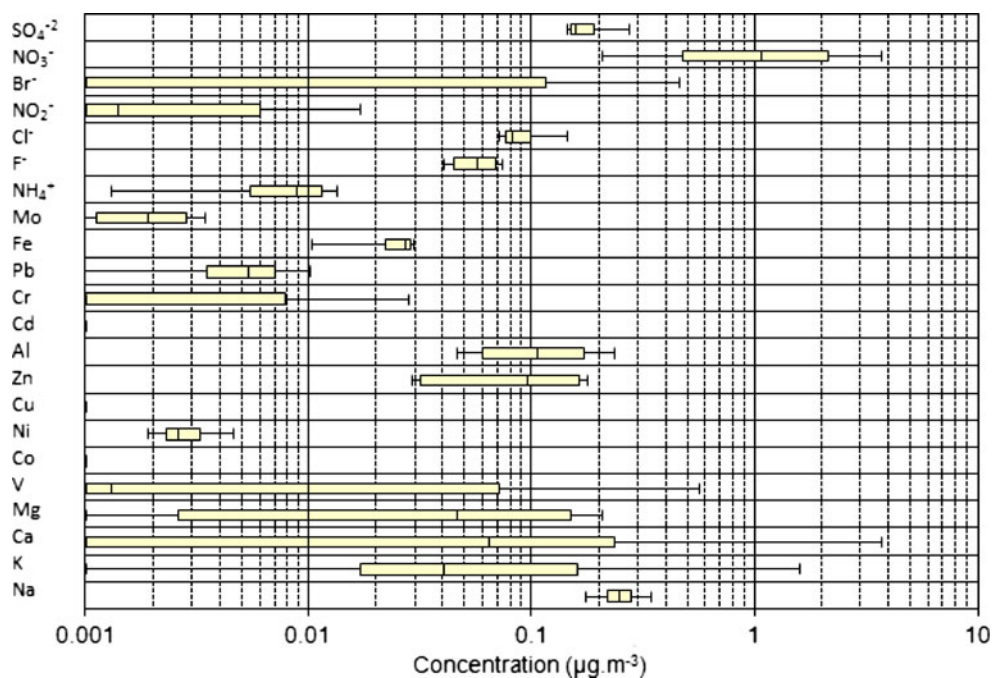


Fig. 6 Box-whisker plot of chemical species of the nighttime samples

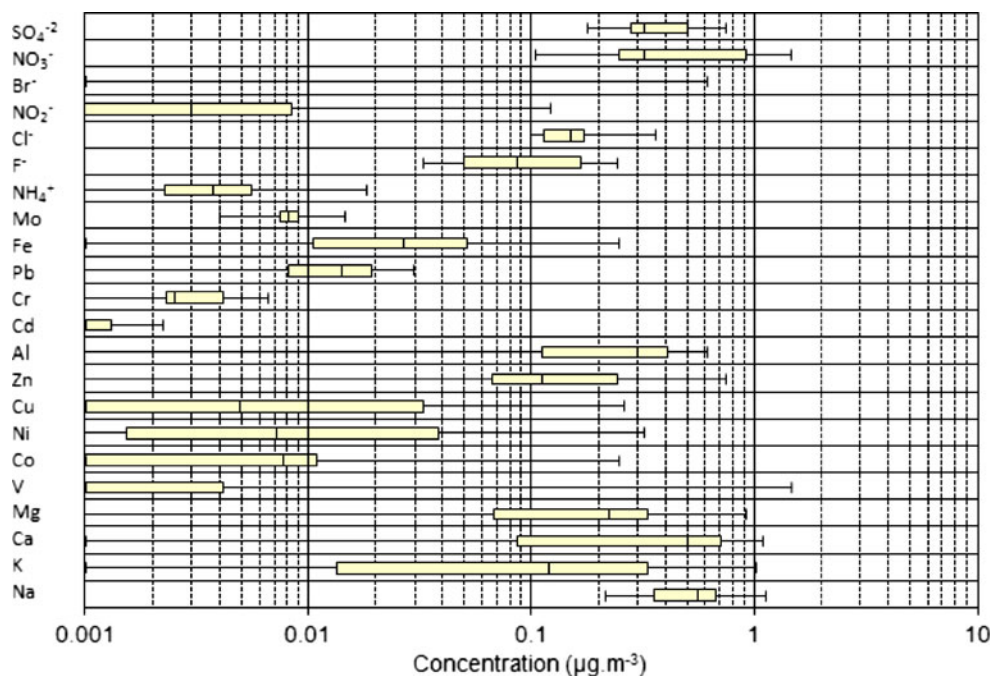


sampling location is 800 m away from the Bosphorus Strait. Dense sea transportation is present through the Strait, which also induces a white cap mechanism. On a concentration basis, although Cl^- and F^- ions have nearly uniform distributions through the stages, a decreasing trend is present from the coarse particle to the fine particle on a percentage basis. This observation suggests that primary sea salt aerosol produced by the mechanical disruption of the sea surface is more dominant than secondary aerosol which is formed by the gas-to-particle conversion (Twomey 1977).

The maximum concentrations of Fe are observed in rush hour samples between the size range of 1.1–4.7 μm . Also, for Cu, higher concentrations were monitored during day-time, between diameters of 0.65 and 0.43 μm . Zn has a nearly uniform distribution throughout the stages, except a slight increase below 3.3 μm .

The maximum elemental composition comprised alkaline and alkaline earth metals, which are Na, K, and Mg, Ca, respectively. Al follows these elements on a concentration basis. The maximum concentrations of these elements were

Fig. 7 Box-whisker plot of chemical species of the rush hour samples



observed in rush hour samples, between 1.1 and 4.3 μm . When long-range dust transportation episodes occur, the concentrations of these elements were raised, especially the iron content with almost threefold.

The proportion of the measured ionic and metallic species is shown as a 3D graph in Fig. 8. These results are stated on a percentage basis of the total aerosol mass. Apparent cumulative mass values are not 100 % because of the unanalyzed portions of aerosols.

Chrysikou et al. (2009) stated that ionic and carbonaceous species are the major constituents of PM in a submicron fraction; subtracting the total ionic content from the PM mass, the carbonaceous material could be estimated. It should also be noted that some other trace elements and trace organic pollutants are all present in the aerosol, but not at a significant amount. Theodosi et al. (2010) executed PM_{10} sampling in Istanbul from November 2007 to June 2009. The sampling location was about 10 km away from our sampling location. Our sampling location is dominantly affected by traffic emissions. In their study, they analyzed the main ions, trace elements, water-soluble organic carbon, and organic (OC) and elemental carbon. According to their results, particulate organic matter and elemental carbon (EC) together account for up to 33 % of the total PM mass.

By considering the undetected part as EC/OC, the estimated EC/OC percentages are about 35–45 % of the total aerosol mass, on average. As expected, the highest EC/OC concentrations are highest in the entire day samples and rush hour samples. Considering the difference in sampling locations, it could be concluded that the results are in harmony.

Less undefined mass component is present when the impactor is set to work at night. In this undefined portion, probable constituents are some trace elements and carbon components. Carbon species comprises the bulk of the undefined portion. If the sampling region and the undefined percentage are investigated well according to the sampling periods, it will be observed that carbon is most probably of traffic origin due to the reduced proportion in the undefined part in the night samples. This hypothesis could be confirmed

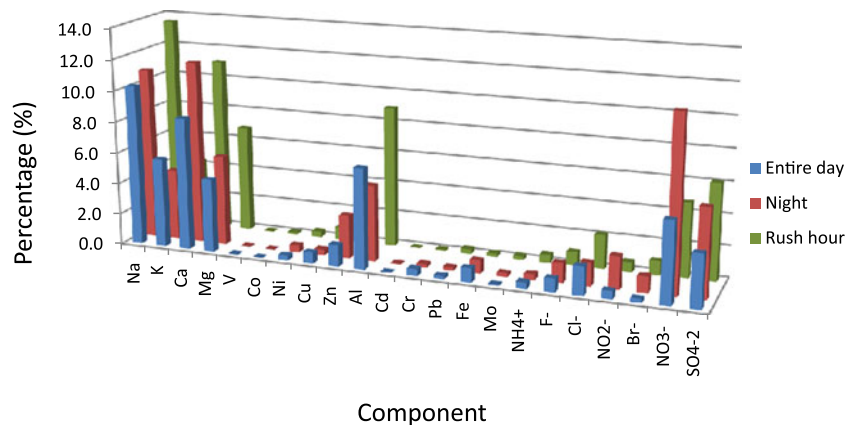
by the shift in the submicron particle concentration. Nearly a threefold decrease is observed in the submicron undefined particle concentration, while other elemental and ionic species increased less or remain nearly the same.

In Turkish NAAQS, only the limit values of Pb, Cd, and Ni elements are present. The lowered lead concentration value on 1 January 2019 is going to be $0.5 \mu\text{g}/\text{m}^3$. This value is not exceeded in any of the samples. Usage of unleaded gasoline helped improve the air quality by decreasing the ambient lead concentration. For Cd and Ni, the threshold values are 5 and $20 \text{ ng}/\text{m}^3$, respectively. But these values are valid from 2020. The mean value for Cd is about $10 \text{ ng}/\text{m}^3$. The minimum value is reached during the night hours. The highest accumulation was observed on the finest particulate matter size, making up half of the total amount. During the rush hour sampling period, Ni was found to be as high as $70 \text{ ng}/\text{m}^3$, while its concentration was lowered to $30 \text{ ng}/\text{m}^3$ during the night, but still not low enough. Ni concentration was found to be slightly higher in the fine mode.

Episodic occasions

During the sampling period, three episodic occurrences were observed. The reason was the long-range dust transportation from the Saharan and Arabian Peninsula. At the time of the transportation, photographs captured by the NASA Earth Observatory (2011) are also exhibited along with the trajectory paths. The HYSPLIT model of NOAA (Air Resources Laboratory; Draxier and Rolph 2012) was run to visualize the air mass transportation during the same time. Altitude had to be given as an input for the model for execution. As also stated in Karaca et al. (2009), there is not an accepted ground-level starting height for the model; rather, different researchers preferred to use diverse altitudes. Lin et al. (2001) chose 1,500 m of elevation, while Dvorska et al. (2009) preferred 750 m. For a long-term fine particle long-range dust transportation, 300 and 500 m were used to reduce topographic effects on the simulations in Liverpool, Australia (Cohen et al. 2011). In a study conducted in

Fig. 8 Percentage of the analyzed species (actual) in aerosol content



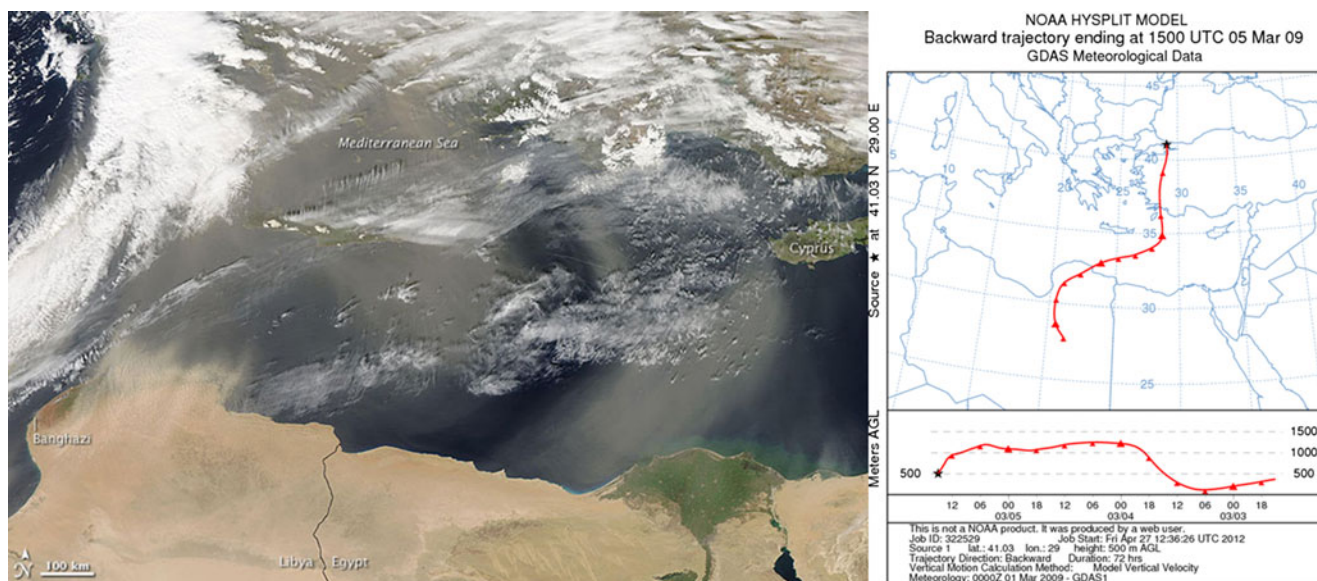


Fig. 9 Episodic event on 06 March 2009

Istanbul by Anil et al. (2009), 1,500 m of elevation was used to run the model; in another study by the same research group, 500 m was used as the aboveground level (Karaca et al. 2009). To overcome this uncertainty, a visual approach was followed in our study. Natural disaster photographs are continuously captured by NASA and published through the web site (<http://earthobservatory.nasa.gov/NaturalHazards/>). The dust trajectory

from the photo and the air mass trajectory from the HYSPLIT model were matched. For the first episodic event, the model was run for different altitudes. A 500-m altitude was found to be the best-fit trajectory. For the other events, a 500-m altitude was selected to simulate the air mass trajectory.

Visual difference was first observed after the sampling period on the filter with a brownish dust layer

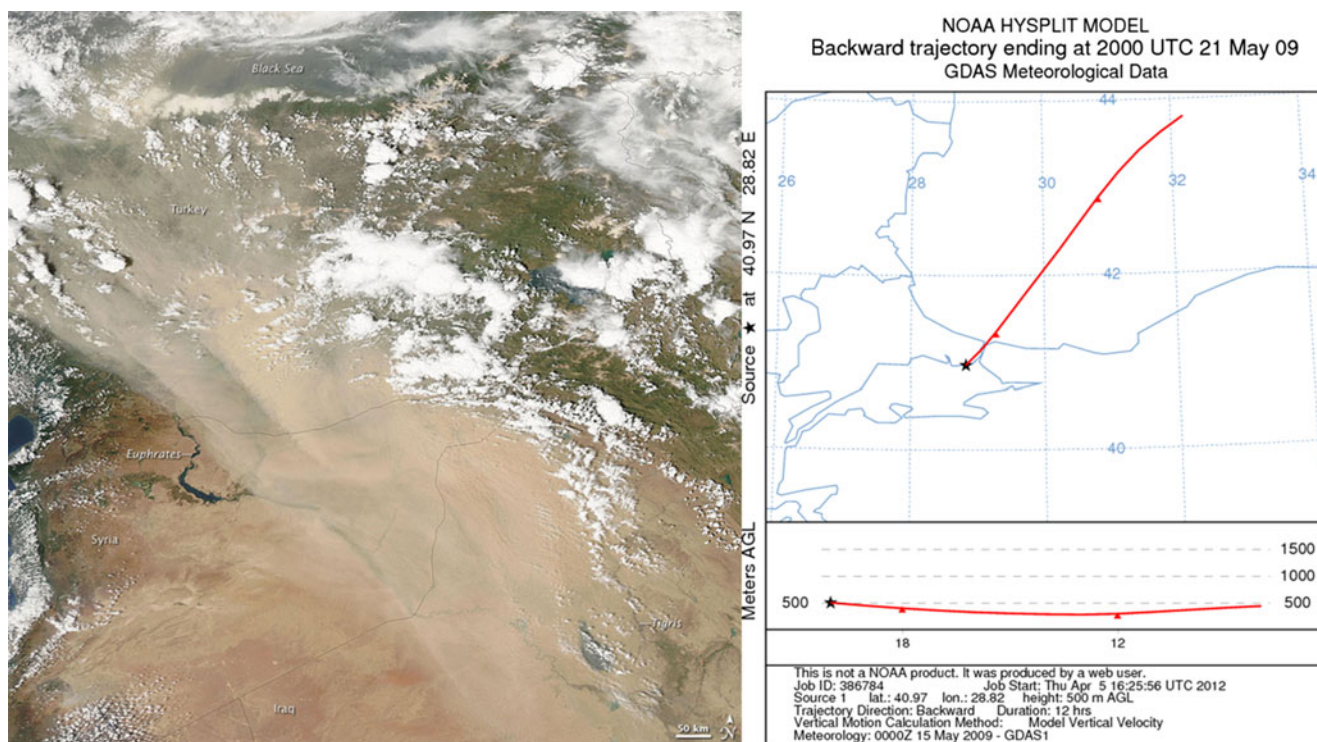


Fig. 10 Episodic event on 21 May 2009

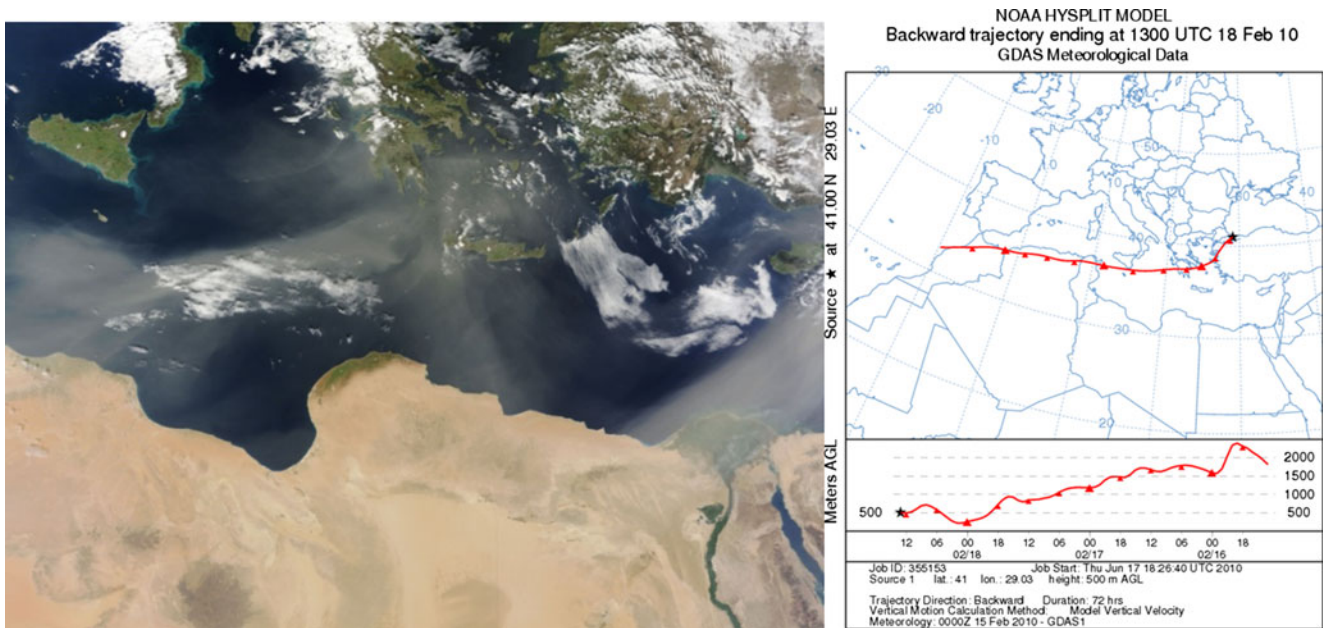


Fig. 11 Episodic event on 18 February 2010

covered instead of a black one. The highest weekly concentration was measured as $92.6 \mu\text{g}/\text{m}^3$ during the first occasion between 04 and 07 March 2009. The photograph and backward trajectory for this episode is shown in Fig. 9. Especially, the Fe concentration was

enriched about threefold; also, Al was the second most enriched element when compared to the entire sampling concentrations. The bulk of the element concentration was accumulated in the fine aerosol size because of the long-range transportation; rainfall was observed as well,

Fig. 12 Log-probability graph for normal period

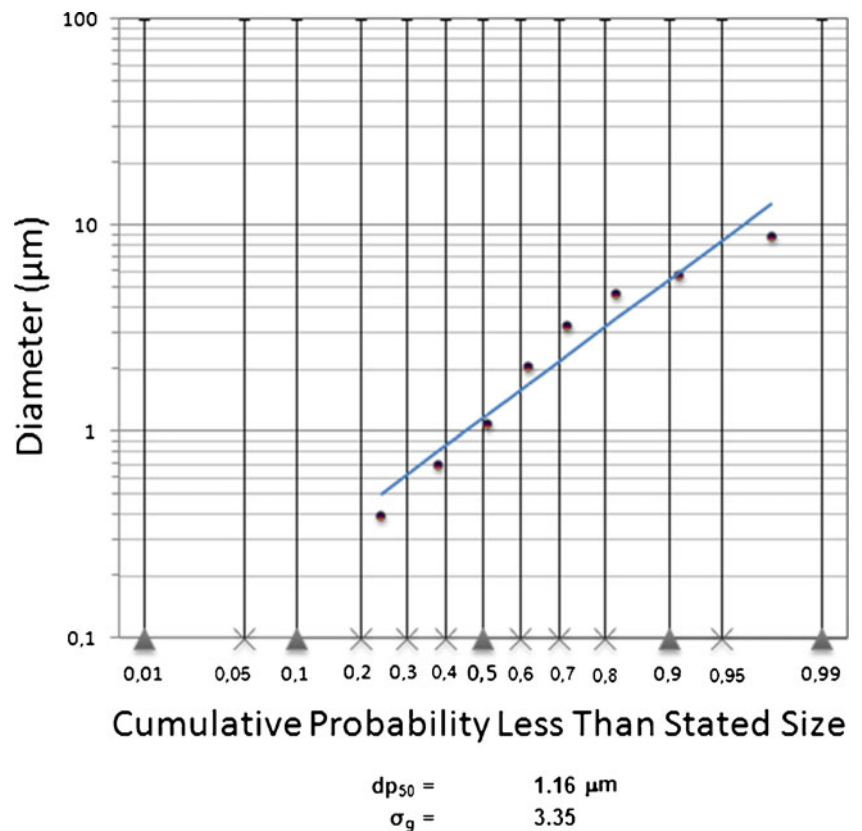
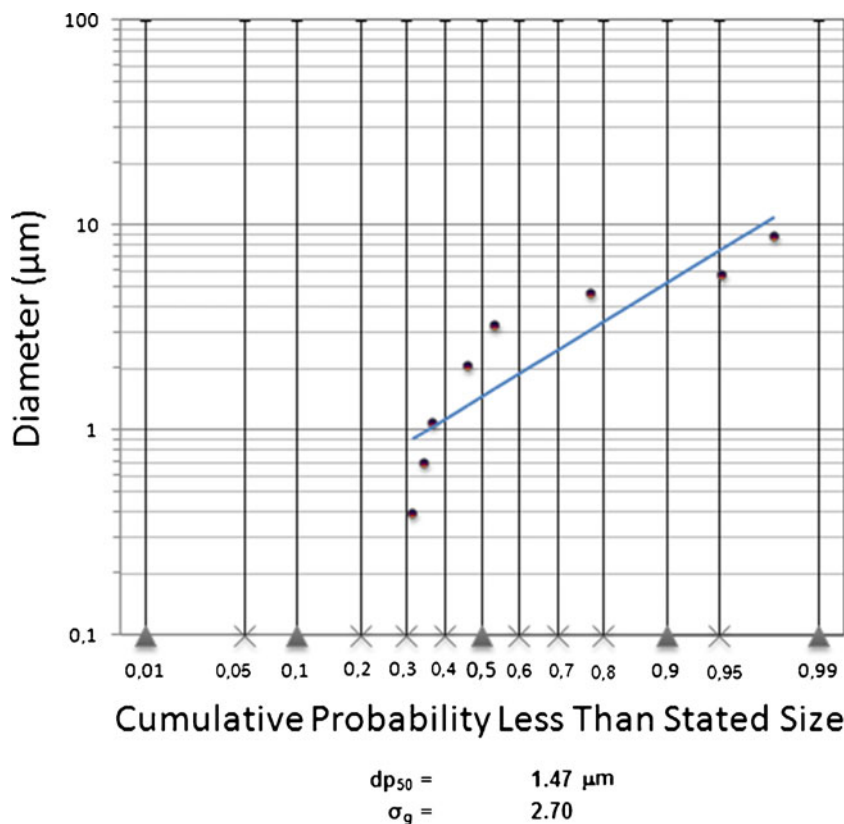


Fig. 13 Log-probability graph for episodic event in March 2009



which acted as a collection mechanism for the coarse aerosol size.

Another episodic event was observed on 21 May 2009. This one had a different route. The transportation occurred from the Arabian Peninsula. Satellite photograph and the HYSPLIT model run are shown in Fig. 10. During this episode, dust storm reached Istanbul over the Black Sea. The HYSPLIT model was run for 12 h, and the trajectory starts where dust in the photo is present in bulk.

The last event occurred on 18 February 2010. As in the first event, transportation occurred from Saharan Desert over the Mediterranean Sea. This episode is shown in Fig. 11.

The episode which occurred in March 2009 was the most effective for the Istanbul atmosphere; the others were not so effective.

Log-probability plots were achieved for all sampling periods. Below, in Figs. 12 and 13, a dominant source shift could also be seen. When Fig. 12 is carefully examined, a normal distribution can be observed. This indicates the ordinary atmospheric state. Figure 13 was prepared to show the size distribution during the dust storm period, which does not fit the log-normal distribution. During this period, fine particles corresponding to $PM_{0.43}$ were increased about 10 %; also, another increase was observed in PM diameters between 3.3 and 4.7 μm due to the Saharan dust transportation.

Conclusion

According to the Air Quality Assessment and Management Regulation, issued on 6 June 2008, PM_{10} and some elemental component evaluations are done. While the threshold value is not exceeded, in 2019, this value is going to be lowered to $50 \mu\text{g}/\text{m}^3$. According to measurement and statistical assessments, the limit value will be exceeded by a 16 % probability. Pb, Cd, and Ni are referred to in the NAAQS. Pb concentrations were lower than the limit value, while excessive Cd and Ni concentrations were observed.

Two major particle modes are found to be present in the Istanbul atmosphere. The fine mode which is between 0.43 and 1.10 μm is of traffic origin, whereas the coarse mode which is between 5.80 and 9.00 μm originated from the mechanical abrasion of the road pavement. Another contribution was from marine aerosol. Observations suggested that primary sea salt aerosol is effective at the coarse particulate mode. Long-range dust transportations were also effective in Istanbul, especially the one observed in spring. The highest weekly ambient PM_{10} concentration was measured as $92.6 \mu\text{g}/\text{m}^3$.

A new trend in the automotive industry is to produce electricity-powered engines. In Turkey, some investments have been made to produce such vehicles. In the near future, by the rise of electrical vehicles, atmospheric particle size distribution and the chemical composition of aerosols are

expected to change. After this realization, new researches are needed to be made on the existing subject to observe the air quality and compositional change and to confirm the results stated in this paper.

Acknowledgment This research has been supported by the Yildiz Technical University Scientific Research Projects Coordination Department (project no. 28-05-02-03). The authors gratefully acknowledge the NOAA Air Resources Laboratory (ARL) for the provision of the HYSPLIT transport and dispersion model and READY website (<http://ready.arl.noaa.gov>) used in this publication. The authors would also like to acknowledge the NASA Earth Observatory for capturing dust storm photographs and for permission for their scientific uses. The authors would like to gratefully thank our beloved departed professor Dr. Ferruh ERTÜRK for his most valuable and most appreciated help and for overseeing this project.

References

- Adachi K, Tainosho Y (2004) Characterization of heavy metal particles embedded in tire dust. *Environ Int* 30:1009–1017
- Al-Khashman OA (2004) Heavy metal distribution in dust, street dust and soils from the work place in Karak Industrial Estate, Jordan. *Atmos Environ* 38:6803–6812
- Anil I, Karaca F, Alagha O (2009) İstanbul’u uzun mesafeli atmosferik taşınım etkilerinin araştırılması: Solunabilen partikül madde epizotları. *Ekoloji* 19(73):86–97
- Brewer R, Belzer W (2001) Assessment of metal concentrations in atmospheric particles from Burnaby Lake, British Columbia, Canada. *Atmos Environ* 35:5223–5233
- Cohen DD, Stelcer E, Garton D, Crawford J (2011) Fine particle characterisation, source apportionment and long-range dust transport into the Sydney Basin: a long term study between 1998 and 2009. *Atmos Pollut Res* 2:182–189
- Cheng MT, Tsai YI (2000) Characterization of visibility and atmospheric aerosols in urban, suburban, and remote areas. *Sci Total Environ* 263:101–114
- Chrysikou LP, Gemenetzi PG, Samara CA (2009) Wintertime size distribution of polycyclic aromatic hydrocarbons (PAHs), polychlorinated biphenyls (PCBs) and organochlorine pesticides (OCPs) in the urban environment: street- vs rooftop-level measurements. *Atmos Environ* 43:290–300
- Dockery DW, Speizer FE, Stram DO, Ware JH, Spengler JD, Ferris BGJ (1989) Effects of inhalable particles on respiratory health of children. *Am Rev Respir Dis* 139:587–594
- Draxler RR, Rolph GD (2012) HYSPLIT (hybrid single particle Lagrangian integrated trajectory) model access via NOAA ARL. NOAA Air Resources Laboratory, Silver Spring, MD. http://ready.arl.noaa.gov/HYSPLIT_traj.php/. Accessed 15 July 2012
- Dvorska A, Lammel G, Holoubek I (2009) Recent trends of persistent organic pollutants in air in central Europe—air monitoring in combination with air mass trajectory statistics as a tool to study the effectivity of regional chemical policy. *Atmos Environ* 43(6):1280–1287
- Fernandez Espinosa AJ, Ternero Rodriguez M, Barragan de la Rosa FJ, Jimenez Sanchez JC (2001) A chemical speciation of trace metals for fine urban particles. *Atmos Environ* 36:773–780
- Finlayson-Pitts BJ, Pitts JN Jr (1993) Atmospheric chemistry of tropospheric ozone formation: scientific and regulatory implications. *JAWMA* 43:1091–1100
- Gustafsson MER, Franzen LG (1996) Dry deposition and concentration of marine aerosols in a coastal area, SW Sweden. *Atmos Environ* 30:977–989
- Harrison RM, Yin J (2000) Particulate matter in the atmosphere: which particle properties are important for its effects on health? *Sci Total Environ* 249:85–101
- Hewitt CN, Jackson AV (2009) Atmospheric science for environmental scientists. Wiley, New York
- Hieu NT, Lee B (2010) Characteristics of particulate matter and metals in the ambient air from a residential area in the largest industrial city in Korea. *Atmos Res* 92:526–537
- Hlavay J, Polyak K, Wesemann G (1992) Particulate size distribution of minerals phases and metals in dusts collected at different workplaces. *Fresenius J Anal Chem* 344:319–321
- Huang X, Olmez I, Aras NK, Gordon GE (1994) Emissions of trace elements from motor vehicles: potential marker elements and source composition profile. *Atmos Environ* 28:1385–1391
- Jacob DJ (1999) Introduction to atmospheric chemistry. Princeton University Press, Princeton
- Karaca F, Anil I, Alagha O (2009) Long-range potential source contributions of episodic aerosol events to PM₁₀ profile of a megacity. *Atmos Environ* 43:5713–5722
- Lin CJ, Cheng MD, Schroeder WH (2001) Transport patterns and potential sources of total gaseous mercury measured in Canadian High Arctic in 1995. *Atmos Environ* 35:1141–1154
- Morawska L, Thomas S, Jamriska M, Johnson G (1999) The modality of particle size distributions of environmental aerosols. *Atmos Environ* 33:4401–4411
- NASA Earth Observatory (2011) <http://earthobservatory.nasa.gov/NaturalHazards/>. Accessed 30 September 2011
- NOAA Air Resources Laboratory (2012) READY Archived Meteorology. <http://ready.arl.noaa.gov/READYmet.php/>. Accessed 15 July 2012
- O’Dowd CD, Smith MH, Consterdine IE, Lowe JA (1997) Marine aerosol, sea-salt, and the marine sulphur cycle: a short review. *Atmos Environ* 31(1):73–80
- Perrino C, Tiwari S, Catrambone M, Torre SD, Rantica E, Canepari S (2011) Chemical characterization of atmosphere in Delhi, India, during different periods of the year including Diwali festival. *Atmos Pollut Res* 2:418–427
- Poschl U (2005) Atmospheric aerosols: composition, transformation, climate and health effects. *Angew Chem Int Ed* 44:7520–7540
- Seinfeld JH, Pandis SN (1997) Atmospheric chemistry and physics: from air pollution to climate change, 1st edn. Wiley, New York
- Theodosi C, Im U, Bougiatioti A, Zampas P, Yenigun O, Mihalopoulos N (2010) Aerosol chemical composition over Istanbul. *Sci Total Environ* 408:2482–2491
- TUIK (Turkish Statistical Institution) (2011) Address based population registration system population census
- Turkish NAAQS (2008) Published on June 6, 2008, print no. 26898
- Twomey S (1977) Atmospheric aerosols. Elsevier, Amsterdam
- Upadhyay N, Majestic BJ, Prapaipong P, Herckes P (2009) Evaluation of polyurethane foam, polypropylene, quartz fiber, and cellulose substrates for multi-element analysis of atmospheric particulate matter by ICP-MS. *Anal Bioanal Chem* 394:255–266
- US EPA (2010) our nation’s air. Office of Air Quality Planning and Standards, Publication No. EPA-454/R-09-002
- Vedal S (1997) Ambient particles and health: lines that divide. *J Air Waste Manag Assoc* 47:551–581
- Whitby KT, Clark WE, Marple VA, Sverdrup GM, Sem GJ, Willeke K, Liu BYH, Pui DYH (1975) Characterization of California aerosols—I. Size distributions of freeway aerosol. *Atmos Environ* 9:463–482
- Wrobel A, Rokita E, Maenhaut W (2000) Transport of traffic-related aerosols in urban areas. *Sci Total Environ* 257:199–211
- Xia L, Gao Y (2011) Characterization of trace elements in PM_{2.5} aerosols in the vicinity of highways in northeast New Jersey in the U.S. east coast. *Atmos Pollut Res* 2:34–44